COLLISIONAL FRAGMENTATION OF ROTATING BODIES.

K.R. Housen, The Boeing Co., MS 2T-50, P.O. Box 3707, Seattle, WA 98124, kevin.r.housen@boeing.com.

Introduction. Many asteroids rotate sufficiently fast that they are at or near the rotational stability limit for a cohesionless material [1-4]. This observation raises a question: does the centrifugal force in a spinning asteroid significantly affect the conditions required for collisional disruption? In principle, a minor collision that would result in simple crater formation on a non-rotating body could disrupt an asteroid spinning near its stability limit. This abstract describes preliminary experiments designed to study the effect of rotation on collisional fragmentation.

Experiments. Two types of spherical targets were manufactured. The first, a simulant of weak rock [5], consists of basalt fragments (50% by weight), fly ash (a binder, 24%), chromite grit (20%) and water (6%). The mixture is placed in a spherical mold to cure for five days then removed from the mold and oven-dried at 90C for two days to remove the water. These targets had diameter=14.7 cm, density=2.2 gm/cm^3, tensile strength=10^6 dy/cm^2 and porosity=21%. The second type of target is weaker and more porous. It consists of quartz sand (17%), Perlite (15%), fly ash (25%) and water (43%), using the same mold, and preparation described above. The resulting material had density=0.4 gm/cm^3, tensile strength=10^5 dyn/cm^2 and porosity=84%.

The impacts occurred under ambient atmospheric pressure in a chamber lined with soft foam. The target rested in a bowl-shaped depression machined into a stiff low-density foam disk (Fig. 1). The foam was fixed to an aluminum disk attached through a spindle to a 0-2000 RPM drive motor. Spheres resting in the foam disk could be spun up to ~370 RPM before instabilities caused them to roll off the fixture. To achieve higher rotational speeds some tests used a small foam cap resting on the top of the target. The top cap could freely rotate and move vertically to minimize interference with target motion after impact. Impact tests with no rotation produced results very similar to those with free-standing targets indicating that the support system for the rotating targets had no significant effect on the results.

The projectiles were cylinders with nominal diameter=6.2 mm and length=6.3 mm. The impact direction was perpendicular to the targets angular velocity vector. Two digital framing cameras running at 4,000 pps recorded the events and provided a measurement of the rotational speed at the time of impact. The initial conditions and results are summarized in Table 1. The maximum internal stress, σ_S, shown in the table is $\sigma_S=(3+\nu)\rho\omega^2R^2/8$, where ν=Poisson's ratio (0.33), ρ=target density, ω=angular velocity (rad/s) and R=target radius.

Results. Figure 2 shows the mass of the largest remaining fragment (ML) normalized by the target mass M for weakly-cemented basalt. Q is the impact kinetic energy/target mass. Symbol labels are the internal stress due to rotation normalized by the target tensile strength, i.e. σ_S/σ_T. Symbols without labels denote non-rotating targets. Surprisingly, rotation significantly reduces the largest fragment size when the rotational stress is as little as 5% of the tensile strength. In this case, Q^*, the specific energy for fragmentation (ML/M=0.5) is nearly a factor of 4 smaller than for non-rotating bodies. Larger values of σ_S/σ_T produce even greater reductions in Q^*.

Results for the porous targets are shown in Figure 3. The porous material was so weak that some fragments broke upon landing on the foam blanket. Cases for which this was observed in the video are shown with an upward arrow to indicate a lower bound on the largest fragment mass. Although there is less data for the porous targets, they too show that rotation reduces the energy needed for disruption.

Conclusion. The degree to which target rotation affects collisional outcomes is surprising. Q^* is approximately proportional to material strength [7]. Hence, one might expect a value of σ_S/σ_T=5% to reduce the effective target strength by about 5%, with a corresponding small change in Q^*. Instead, rotation causes Q^* to drop by a factor of four. The reason for this sensitivity is not fully understood. One possibility is that the impact shock weakens the target enough that, while a non-rotating body would remain coherent, the rotational stresses are then sufficient to disrupt the weakened target.

Note that σ_S/σ_T=5% corresponds to an angular speed about a factor of 5 below the stability limit. The present results indicate a significant reduction in the energy required for fragmentation in this case. Therefore, rotation could significantly reduce the collisional lifetime of asteroids whose spin rates are within a factor of several of the stability limit.

Finally, until the mechanism responsible for the strong dependence on rotation is understood, the extension of these results to gravity-dominated asteroids is uncertain. For example, if strength-degradation by the shock is responsible, rotation may have only a small affect on the disruption of gravity-dominated asteroids. This question will be addressed in further experiments and in numerical simulations.

References: [1] Harris A.W. (1996) LPSC XXVII, 493-494; [2] Holsapple K. (2001) *Icarus* **154**, 432-448; [3] Pravec P. *et al* . (2002) Asteroids III, 113-122; [4] Holsapple K. (2002) Workshop Proc: *Scientific Requirements for Mitigation of Hazardous Comets and Asteroids* ; [5] Housen K. *et al*. (1991) *Icarus*, **94**, 180-190. [6] Housen K. (1993), LPSC XXIV. [7] Davis D. and Ryan E. (1990) *Icarus*, **83**, 156-182.

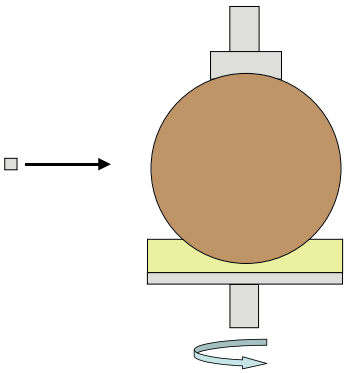

Figure 1. Fixture for rotating-target experiments.

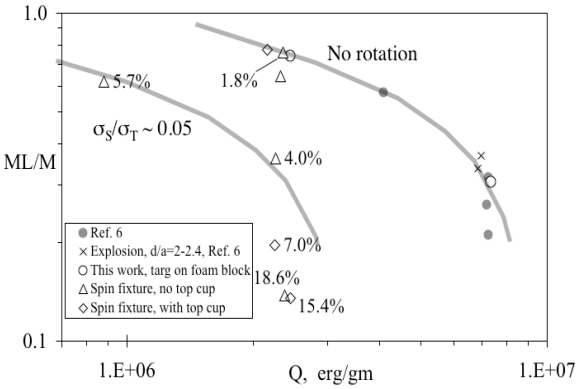

Figure 2. Results for weakly-cemented basalt.

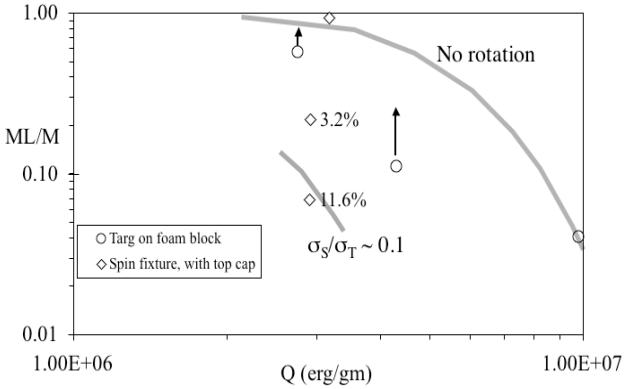

Figure 3. Results for porous targets.

Table 1

ID	σ_T	ω	σ_S	σ_S/σ_T	IT	Vel	M	ML	$Q/10^6$	ML/M	Remarks
-	cgs	rpm	cgs	–	-	km/s	(gm)	(gm)	erg/gm	-	–
Weakly cemented basalt targets											
1852	4.82E+05	0	0	0	1	1.84	3766	2790	2.44	0.74	No-rotation. Target on foam block.
1855	7.14E+05	0	0	0	3	1.50	3452	1054	7.36	0.31	No-rotation. Target on foam block.
1868	6.38E+05	0	0	0	1	1.77	3666	2357	2.32	0.64	Targ in bot cup. No top cap used.
1870	1.35E+06	0	0	0	1	1.71	3682	2850	2.16	0.77	No-rotation. Small top cup. Compare 1868.
1881	1.31E+06	0	0	0	1	1.75	3852	2970	2.16	0.77	Shot in spin fixture at zero RPM
1869	1.43E+06	215	2.64E+04	0.02	1	1.83	3868	2940	2.35	0.76	Rotating. No top cup.
1875	1.04E+06	277	4.16E+04	0.04	1	1.75	3686	1326	2.26	0.36	Rotating. No top cup.
1864	3.01E+05	324	5.59E+04	0.19	1	1.78	3618	500	2.38	0.14	Rotating. No Top cup.
1874	1.26E+06	353	7.20E+04	0.06	1	1.13	3926	2431	0.88	0.62	Top cup used.
1873	1.58E+06	438	1.11E+05	0.07	1	1.80	3924	770	2.24	0.20	Top cup used. Target not oven dried.
1871	1.35E+06	619	2.07E+05	0.15	1	1.79	3658	495	2.38	0.14	Top cup used.
Porous low-density targets											
1854	9.99E+04	0	0	0	1	1.87	969	39.3	9.81	0.04	No rotation. Target on foam block
1856	7.99E+04	0	0	0	2	1.56	682	76.2	4.30	0.11	No rotation. Target on foam block
1857	7.11E+04	0	0	0	2	1.26	696	399	2.75	0.57	No rotation. Target on foam block
1877	2.41E+05	0	0	0	2	1.52	862	803	3.17	0.93	No rotation. High-strength target.
1860	6.57E+04	152	2.11E+03	0.03	2	1.23	620	135	2.91	0.22	Top cup used.
1859	6.66E+04	288	7.68E+03	0.12	2	1.23	629	43.5	2.90	0.07	Top cup used.
1867	5.01E+04	873	6.69E+04	1.33	–		590			0	No proj. Target ruptured at 873 RPM.

IT = imp type: [1] 2024-T4 alum, 0.543 gm, 2.8 gm/cc; [2] Lexan, 0.240 gm, 1.24 gm/cc; [3] Lead, 2.26 gm, 11.4 gm/c
σ_T= targ tens strength; ω = targ rot rate; σ_S=spin stress; M=targ mass; Q=kinetic energy/M; ML=largest frag mass